Nanoscale Advances

ROYAL SOCIETY OF CHEMISTRY

PAPER

Cite this: *Nanoscale Adv.*, 2022, **4**, 447

Bioinspired photo-crosslinkable self-assembling peptides with pH-switchable "on–off" luminescence†

Raffaele Pugliese,*[ad] Monica Montuori[c] and Fabrizio Gelain *[ab]

Significant progress has been made in peptide self-assembly over the past two decades; however, the *in situ* cross-linking of self-assembling peptides yielding better performing nanomaterials is still in its infancy. Indeed, self-assembling peptides (SAPs), relying only on non-covalent interactions, are mechanically unstable and susceptible to solvent erosion, greatly hindering their practical application. Herein, drawing inspiration from the biological functions of tyrosine, we present a photo-cross-linking approach for the *in situ* cross-linking of a tyrosine-containing LDLK12 SAP. This method is based on the ruthenium-complex-catalyzed conversion of tyrosine to dityrosine upon light irradiation. We observed a stable formation of dityrosine cross-linking starting from 5 minutes, with a maximum peak after 1 hour of UV irradiation. Furthermore, the presence of a ruthenium complex among the assembled peptide bundles bestows unusual fluorescence intensity stability up to as high as 42 °C, compared to the bare ruthenium complex. Also, due to a direct deprotonation–protonation process between the ruthenium complex and SAP molecules, the fluorescence of the photo-cross-linked SAP is capable of exhibiting "off–on–off–on" luminescence switchable from acid to basic pH. Lastly, we showed that the photo-cross-linked hydrogel exhibited enhanced mechanical stability with a storage modulus of ~26 kPa, due to the formation of a densely entangled fibrous network of SAP molecules through dityrosine linkages. As such, this ruthenium-mediated photo-cross-linked SAP hydrogel could be useful in the design of novel tyrosine containing SAP materials with intriguing potential for biomedical imaging, pH sensing, photonics, soft electronics, and bioprinting.

Received 15th September 2021
Accepted 19th November 2021

DOI: 10.1039/d1na00688f

rsc.li/nanoscale-advances

1. Introduction

Self-assembling peptides (SAPs) have gained considerable attention because of their potential applications in biology, nanotechnology, tissue engineering, and regenerative medicine.[1–4] Rationally designed SAPs can self-assemble into various nanostructures (*i.e.* nanofibers, nanotubes, nanospheres, nanorods, and plate-like crystals).[5] These structures with high water content (~99%) and a high density of functional groups (namely bioactive motifs) may act as versatile scaffolds and provide various affinities for material manipulation.[6]

Transient non-covalent interactions determine the final morphology of SAPs, which can be controlled by varying the sequence of amino acids or the peptide concentration (when in solution), or by manipulating the environmental parameters (*e.g.* temperature, solvents, or ionic strength); as such, these changes can alter the self-assembling kinetics, pore size, final conformation of entangled nanostructures, and the density of bioactive functional motifs (if present).[7–9]

In contrast, covalent cross-linking after self-assembly using irreversible bonds would lead to more robust and stable structures.[10–12] However, lack of self-error correcting mechanism during the linking process is perhaps the reason why direct formation of irreversible covalent bonds has not been widely attempted for well-defined nanostructures. Moreover, covalent cross-linking may interfere with the self-assembly process of the hydrogelator and result in dehydrogelation. Thus, a promising strategy to overcome this issue is to modulate the self-assembly process, followed by the covalent stabilization of the formed nanostructures; the non-covalent self-assembly first controls the nanostructure formation, while subsequent covalent bond formation stabilizes such structures.[11] The success of this

[a]*Tissue Engineering Unit, Institute for Stem Cell Biology, Regenerative Medicine and Innovative Therapies-ISBReMIT, Fondazione IRCCS Casa Sollievo della Sofferenza, 71013 San Giovanni Rotondo, FG, Italy. E-mail: f.gelain@css-mendel.it*

[b]*Center for Nanomedicine and Tissue Engineering (CNTE), ASST Grande Ospedale Metropolitano Niguarda, 20162 Milan, Italy*

[c]*Biotechnology and Biosciences Department, University of Milano-Bicocca, 20162 Milan, Italy*

[d]*NeMO Lab, ASST Grande Ospedale Metropolitano Niguarda, 20162 Milan, Italy. E-mail: raffaele.pugliese@nemolab.it*

† Electronic supplementary information (ESI) available: Fig. S1: Temperature-dependent fluorescence intensity of the peptide moiety; Fig. S2: mechanical properties of the 33Y and 33Y photo-cross-linked peptides. See DOI: 10.1039/d1na00688f

process requires that the reaction conditions must not disturb the self-assembly phenomenon, and the covalent linking must not negatively influence the scaffold's self-assembled nanoarchitecture. Furthermore, it is necessary to use cross-linking or photo-cross-linking agents that do not interfere with the final biocompatibility and functionality of the scaffold. Finally, achieving specific cross-linking sites is another key aspect to keep in mind for this approach.[13]

Over the past few years, various processing methods and cross-linking techniques proved to be valuable tools for covalent linking of SAP-based materials, providing excellent improvements of their chemical–physical and biomechanical properties.[11,14–23]

For instance, Hartgerink and his team reported the use of covalent capture of collagen mimetic peptides (CMPs), through the formation of isopeptide bonds between lysine and either aspartate or glutamate, using carboxylate activating reagents 1-ethyl-3-(3-(dimethylamino)propyl)carbodiimide (EDC) and hydroxybenzotriazole (HOBt).[24,25] By using a similar approach, our laboratory reported the design of covalent capture of SAP-hydrogel using a one-pot *in situ* gelation system, based on EDC/*N*-hydroxysulfosuccinimide (sulfo-NHS) coupling, to readily cross-link LDLK12 molecules, in order to tune its biomechanics without affecting the spontaneous formation of β-sheet-containing nanofilaments.[16] In addition, we demonstrated how genipin cross-linking can also be adopted with a number of different lysine-containing SAPs (linear, mixed, branched, biotinylated, and functionalized) to produce nanofibrous networks with increased mechanical properties ($G' \geq 0.2$ MPa), thermostability (≥100 °C) and optical properties, paving the way for novel optoelectronic and photonic applications of cross-linked SAPs.[15]

Dityrosine cross-linking draws considerable interest because of its distinctive properties such as outstanding elasticity and intrinsic fluorescence.[26] Further, dityrosine bonds are a key component of many natural materials in their native tissues: indeed tyrosine cross-links stabilize proteins in numerous structural tissues.[27] The sea urchin egg, for example, utilizes tyrosine cross-linking during fertilization, yielding a membrane structure harder and more resistant to physical deformation and proteolysis digestion.[28] Dityrosine cross-linking has also been detected in resilin extracted from desert locusts and dragonflies, which contributes to the exceptional jumping abilities of these species.[29] Also, in order to protect themselves during development, aquatic caddisfly larvae build composite shelters from adhesive silk fibers, stones, and organic materials collected from their environment through dityrosine bonding.[30,31]

Drawing inspiration from natural living systems, in order to expand the tool kits for the covalent capture of supramolecular SAP hydrogels and improve their chemical–physical and biomechanical features, we developed and validated a photo-cross-linking approach for the *in situ* cross-linking of a tyrosine-containing LDLK12 peptide (Ac-YYGGGLDLKLDLKLDLK, dubbed 33Y). This approach is based on the well-established ruthenium catalyzed (in the presence of ammonium persulfate) photo-cross-linking reaction of two tyrosine residues in close proximity to each other to give dityrosine adducts, under visible light. Ruthenium is an efficient visible light-harvesting molecule, which donates an electron to the persulfate upon excitation, resulting in the cleavage of the O–O bond. The products are Ru(III), an electron oxidant, and a sulfate radical. Ru(III)-mediated formation of a tyrosyl radical is proposed as an initiating step. Coupling of this radical with one of several possible nucleophiles (*e.g.* another tyrosine residue in close proximity) and the subsequent removal of a hydrogen atom by the sulfate radical completes the reaction.[32]

By positioning the reactive sites outside the self-assembling backbone of the 33Y peptide sequence, we managed to prevent interference between the self-assembling and photo-cross-linking processes. As a result, we demonstrated that ruthenium specifically reacts with 33Y pre-assembled nanostructures. The dimerization of tyrosine residues among peptide bundles was verified by UV-vis absorbance and fluorescence emission. In addition, ruthenium photo-cross-linking enhanced the mechanical stability of the hydrogel with a storage modulus of ~26 kPa. Another intriguing observation ascribable to the direct electron transfer between the ruthenium complex and SAP molecules is that the fluorescence of the photo-cross-linked SAP "turns off" (in acid solution) and "turns on" (in basic solution), generating a pH-switchable on–off system.

We anticipate that this strategy could potentially be useful for other tyrosine-containing SAPs, by improving their fluorescence, biomechanical, and optoelectronic properties to suit the needs of different applications in bioimaging, photonics, tissue engineering, and beyond.

2. Results and discussion

2.1 Design and evidence of a photo-cross-linkable peptide

Biomimetic LDLK12-based assembling peptides have been extensively studied, and have shown promise as a platform for the regeneration of the injured spinal cord,[33,34] cartilage,[35] and nucleus pulposus.[36] LDLK12 efficiently self-assembles into nanofibers (with 10–20 nm diameter) and rapidly changes into a three-dimensional porous supramolecular hydrogel with high water content (from 96% to 99.5%) under physiological conditions. In addition, it can be feasibly functionalized with short epitopes at one or both termini to obtain biomimetic scaffolds customized for specific applications.[37–40] Further, it is amenable of multiple ramifications, connected with one or multiple "N_α,N_ε-di-Fmoc-lysine knots", which can be mixed (at different molar ratios) with linear SAPs before self-assembling in order to increase the stiffness of the SAP hydrogels without affecting their secondary β-sheet structure.[41]

Starting from this background, we added two tyrosine residues to the N-terminus of LDLK12 to produce photo-cross-linkable peptide Ac-YYGGGLDLKLDLKLDLK-$CONH_2$ (dubbed 33Y). To avoid the crosstalk between the assembly of LDLK12 and tyrosine cross-links, we introduced a three-glycine spacer between the LDLK12 backbone and tyrosine residues. The glycine linker serves as a spacer to disconnect the geometric constraints of dityrosine cross-links from the self-assembling LDLK12 backbone, as previously reported.[42]

The 33Y peptide was dissolved in distilled water (pH 5.5) to achieve a final concentration of 1% (w/v), and incubated overnight at +4 °C in order to guarantee the spontaneous formation of pre-assembled nanofibers. Afterwards, we mixed the desired amounts of $Ru(bpy)_3Cl_2$ and APS with the pre-assembled 33Y (see the Materials and methods for further details) and irradiated the mixture with UV-light to initiate the photo-cross-linking (Fig. 1a). To study the formation of dityrosine cross-links among the assembled 33Y peptide bundles, we investigated the photo-cross-linking of a set of 33Y peptides subject to different irradiation time courses (*i.e.* 5, 10, 15, 20, 25, and 60 min) in the presence of $Ru(bpy)_3Cl_2$ and APS, by UV-vis absorbance and fluorescence spectroscopy. As shown in Fig. 1b, upon light irradiation, a major peak of tyrosine centered at 276 nm gradually red-shifted to 286 nm, which corresponds to the absorbance of dityrosine (indicated by the grey arrow); this is because the formation of dityrosine cross-linking further delocalizes the electrons on the aromatic rings, leading to the red shift in the UV absorbance.[43] Notably, we observed a stable formation of dityrosine cross-linking after 5 minutes of photo-irradiation (cyan line), with a maximum peak after 1 hour of UV irradiation (dark green line). Furthermore, the formation of a peak at ~450 nm is clearly visible, due to the presence of the ruthenium complex within the peptide bundles (not present in the wild type 33Y peptide, dark line). In contrast, in the fluorescence spectra of photo-cross-linked 33Y peptides (Fig. 1c), two emission peaks located at 430 nm and 675 nm appeared (excited at 280 nm), which are characteristic of the dityrosine moiety and ruthenium complex, respectively. In this case we observed the maximum fluorescence intensity at 20 min. There were no fluorescence peaks at 430 nm and 675 nm for the 33Y wild type (dark line), confirming the assumption that such emission peaks are related to the photo-cross-linking reaction. As expected, the fluorescence images confirmed that photo-cross-linked 33Y showed high fluorescent emission in the visible region (Fig. 1d), exhibiting crystal-like structures similar to those reported by Gazit *et al.* with diphenylalanine-derivative peptides,[44] useful as photo-luminescent assemblies for power generation.[45]

2.2 Thermal stability of the luminescent photo-cross-linked peptide

Since the fluorescence of several dyes presents a strong dependence on temperature, hampering their practical applications in temperature sensing/imaging,[46,47] we next evaluated the temperature-dependent fluorescence intensity. Indeed, the development of temperature sensors at the nano- and micro-scales has recently received considerable attention due to the growing interest in performing measurements on a variety of unconventional systems, *e.g.*, cells, lab-on-a-chip, and microfluidic devices.[48]

As already reported,[49–52] the excited Metal-to-Ligand Charge Transfer (MLCT) state of bare $Ru(bpy)_3Cl_2$ decays with temperature increments. Therefore, the fluorescence of the free aqueous ruthenium complex decreases with increasing temperature. As expected, we observed a drastic decrease in the intensity of the emission peak of the bare ruthenium complex in a linear fashion ($r^2 = 0.99$) in the range of 20–42 °C (Fig. 2a), a relevant temperature range for biological systems. Surprisingly, the entrapped $Ru(bpy)_3Cl_2$ among photo-cross-linked 33Y peptide bundles retains its photo-luminescent properties up to 42 °C (Fig. 2b) and even after several heating cycles (data not shown). No fluorescent decay was observed for the peptide moiety (emission peak at 430 nm, Fig. S1†).

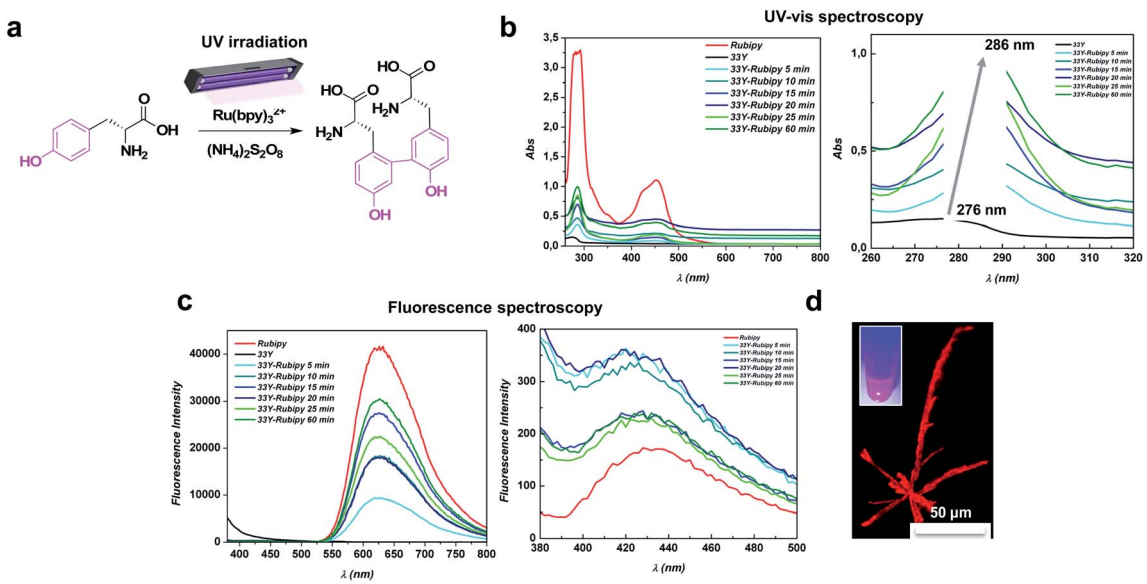

Fig. 1 (a) Schematic of ruthenium-complex-catalyzed conversion of tyrosine to dityrosine upon light irradiation. (b) UV-vis spectra of the dityrosine formation among 33Y assembled bundles upon different irradiation time courses; the increasing redshift at 286 nm corresponds to the absorbance of dityrosine cross-linking. (c) Fluorescence spectra of photo-cross-linked 33Y peptides with excitation at 280 nm; the photo-cross-linked 33Y peptides showed two emission peaks located at 430 nm and 675 nm, which are characteristic of the dityrosine moiety and ruthenium complex among peptide bundles. (d) Fluorescence images of photo-cross-linked 33Y exhibiting crystal-like structures.

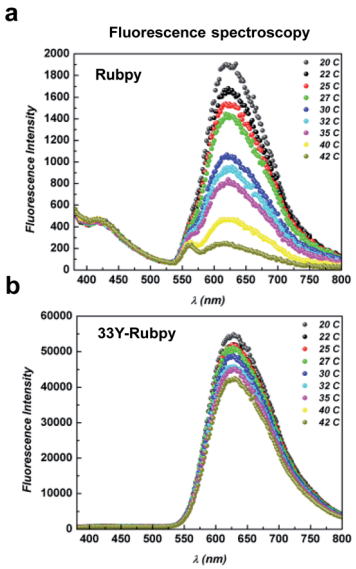

Fig. 2 Temperature-dependent fluorescence intensity of (a) bare ruthenium and (b) entrapped ruthenium among photo-cross-linked 33Y peptides. A drastic decrease of the intensity of the emission peak of the bare ruthenium complex was observed in the range of 20–42 °C, while ruthenium among photo-cross-linked 33Y peptides retains its photo-luminescent properties up to 42 °C.

Overall, these data demonstrate that the ruthenium complex entrapped in the photo-cross-linked 33Y SAP retains its photo-physical properties compared to the free complex, and that the temperature dependence of fluorescence can be exploited to develop thermo-stable devices at the nano-scale level.

2.3 pH-switchable on–off system

Since pH plays a key role in regulating many cellular metabolic pathways, and it is also a fundamental input signal in making sensing, switching, and logic molecular devices, we explored whether the photo-cross-linked 33Y features pH-induced "on–off" emission-switching properties. In this endeavor we selected the photo-cross-linked 33Y peptide with the highest emission intensity value (*i.e.* after 1 hour of UV irradiation), to which a desired volume of different pH buffers (pH 2–14, see the Materials and methods for further details) has been added before assessing its UV-vis absorbance and fluorescence properties (Fig. 3a and b). At acidic pH 2 to 4 (green and purple lines), we observed low values of emission peaks located at 430 nm (fluorescence off). In contrast, pH 6 featured a sharp intensity increase for the band at 430 nm (cyan line, fluorescence on). A third state of low value fluorescence intensity was observed upon increasing the pH from 8 to 10 (lines light-green and orange, fluorescence off). Lastly, pH 12 (yellow line) exhibited a high fluorescence intensity similar to that of pH 6, while pH 14 showed a slight decrease of the fluorescence band at 430 nm (fluorescence on).

The above-mentioned four luminescence "on–off" states are reported in Fig. 3c and S2,† thus confirming the propensity of the photo-cross-linked SAP to have "off–on–off–on" luminescence switchable from acid to basic pH. Notably, as previously reported on other ruthenium-based complexes, this "on–off" emission switching could be associated with the deprotonation–protonation processes among the ruthenium complex at different pH values.[53] In brief, the imidazole rings uncoordinated to the ruthenium can exhibit three independent ground-state protonation/deprotonation processes at different pH values with a transition from the state $[Ru(bpy)_3]^{2+}$ to the state $[Ru(bpy)_3]^{4+}$ (+2H), or to the state $[Ru(bpy)_3]^{5+}$ (+1H) and *vice versa*.[54–57] Overall, this exciting property gained from the photo-cross-linked SAP makes it a promising tool for advanced optical display and/or sensing.

2.4 Changing the photo-physical properties of the ruthenium complex

As it is well known that sulfuric acid (H_2SO_4) can influence the absorbance and fluorescence emission of the ruthenium complex by modifying the MLCT transition to different states,[58] we added H_2SO_4 to the bare $Ru(bpy)_3Cl_2$ (see the Materials and methods for further details) to evaluate whether this change can influence the photo-cross-linking and the luminescence "on–off" emission-switching properties. As shown in Fig. 4a, the $Ru(bpy)_3Cl_2$–H_2SO_4 (dark green line) exhibited a shift of the absorbance emission peak to 700 nm, compared to the $Ru(bpy)_3Cl_2$ wild-type (peak at 450 nm, light green line), as well as for the fluorescence spectrum in which the emission peak is located at 589 nm (Fig. 4b), thus resulting in a change of electroluminescence color.

Hence, we subjected the 33Y peptide to photo-cross-linking with the $Ru(bpy)_3Cl_2$–H_2SO_4 complex (1 hour under UV-light), and, subsequently, to different pH buffers to test the pH-induced "on–off" emission-switching properties (Fig. 4c). Again, we observed four luminescence "on–off" steps (purple line), which appeared to be similar to those of the unmodified photo-cross-linked 33Y peptide (blue line). Indeed, pH 2 featured high values of the emission peak at 430 nm (fluorescence on). In contrast, low fluorescence intensity was detected upon increasing the pH from 4 to 8 (fluorescence off). Instead, a sharp intensity increase of fluorescence was seen at pH 10 (fluorescence on). Lastly, pH 12 exhibited again low fluorescence intensity, while at pH 14 a slight increase of the fluorescence band at 430 nm was seen (fluorescence off).

It is worth noting that exhibiting luminescence at extremely acidic pHs may be useful for applications in tumor cell detection or glial scar formation following acute spinal cord injury. Overall, the ability to modulate the "off–on–off–on" and "on–off–on–off" pH-induced luminescence using the same photo-cross-linked peptic system obliterates any ambiguity from the detected signal coming from a set of unmodified and sulfuric acid-treated photo-cross-linked 33Y peptides and, as such, may pave the way for the development of miniaturized optical sensors entirely made of SAPs that can be feasibly integrated into lab-on-a-chip detection devices.

2.5 Mechanical stability and nanostructure of the photo-cross-linked peptide hydrogel

Finally, we investigated the mechanical properties and the nano-morphology of photo-cross-linked 33Y by rheology and atomic force microscopy (AFM), respectively.

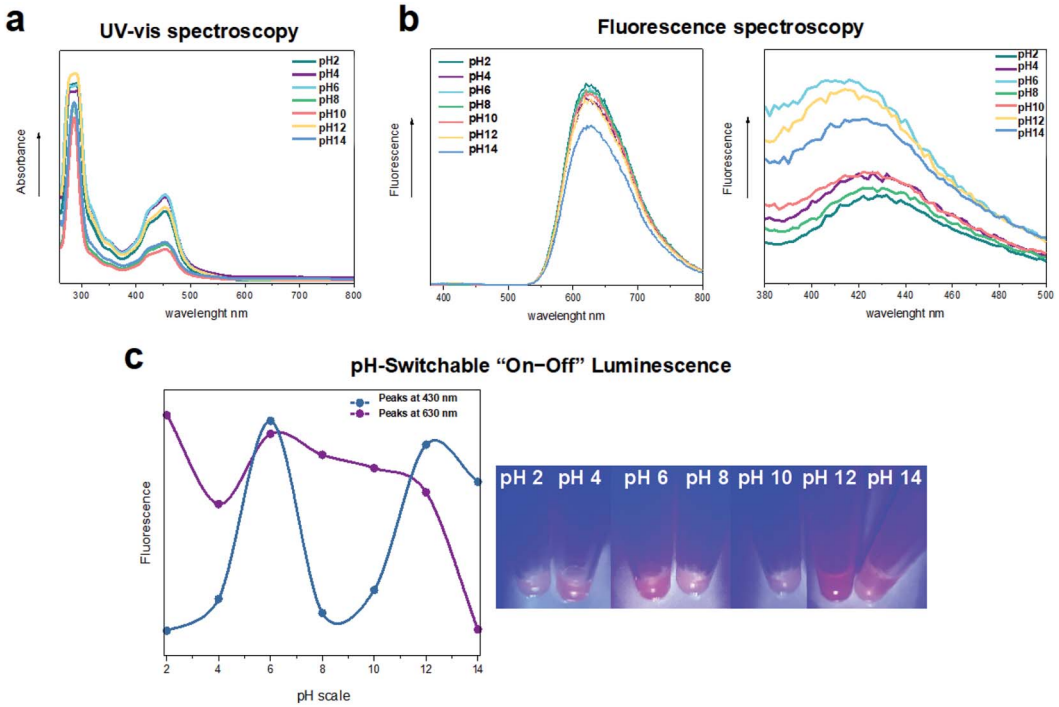

Fig. 3 (a) UV-vis absorbance and (b) fluorescence spectroscopy of the photo-cross-linked 33Y peptide after 1 hour of UV irradiation with different pH buffers. (c) "Off–on–off–on" luminescence switchable from acid to basic pH of the photo-cross-linked 33Y peptide, and images of the photo-cross-linked 33Y peptide under UV light (λ ~395 nm) at different pHs.

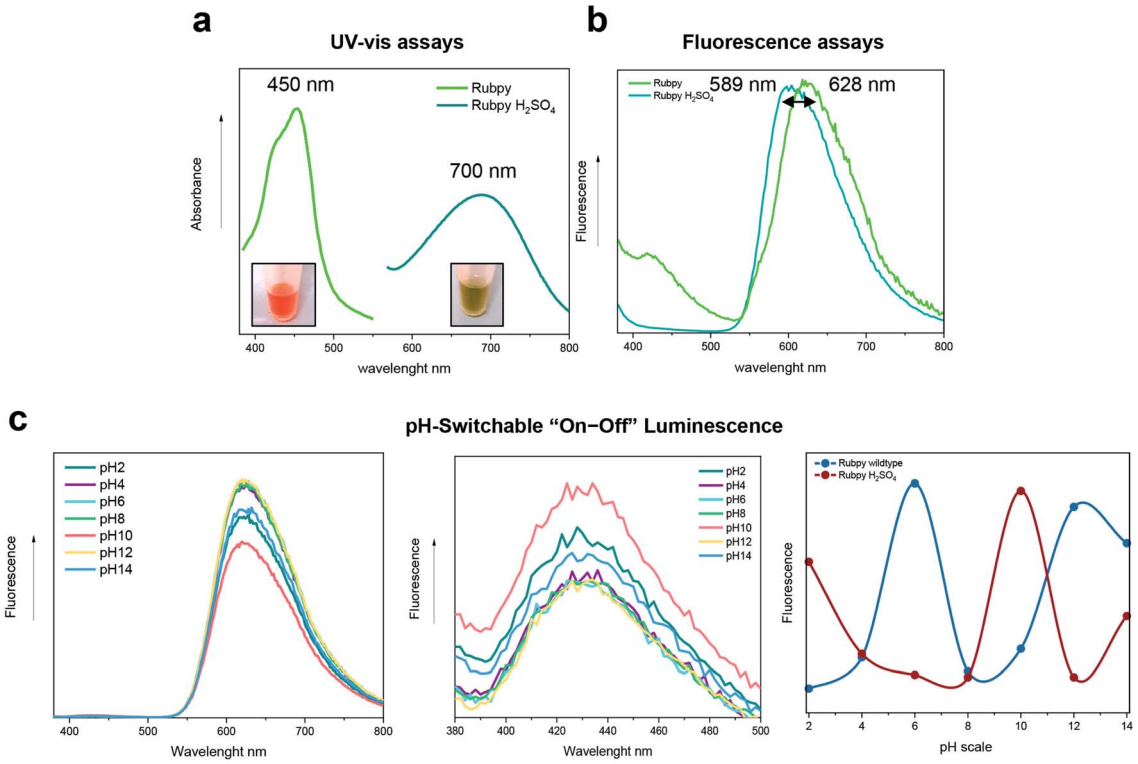

Fig. 4 Ruthenium modified with sulfuric acid showing a shift of the absorbance emission peak to 700 nm (a) and the fluorescence emission peak to 589 nm (b) compared to the ruthenium wild type, thus resulting in a change of electroluminescence color. (c) "On–off–on–off" pH-induced luminescence using a 33Y photo-cross-linked peptic system pre-treated with sulfuric acid.

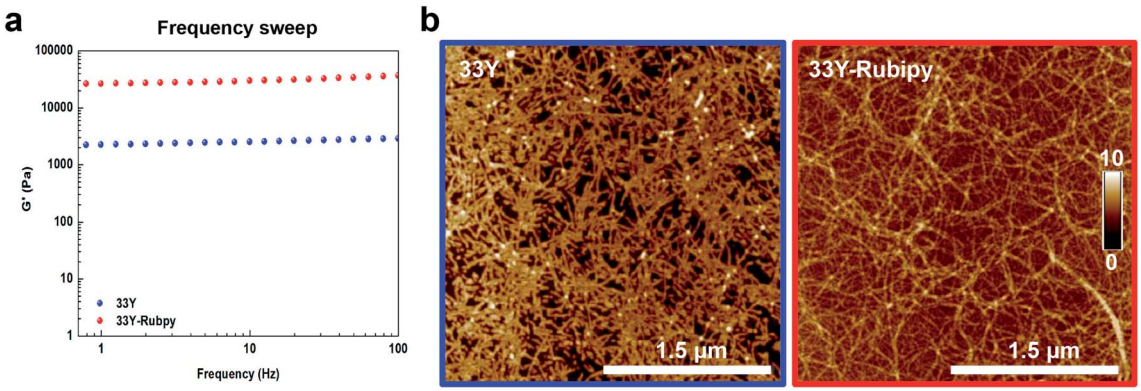

Fig. 5 (a) Frequency sweep (0.1–100 Hz, fixed strain 1%) of 33Y and 33Y photo-cross-linked peptides. 33Y displayed a G' value of 2 kPa, while photo-cross-linked 33Y showed an increase in the storage modulus throughout the tested frequency range, with G' equal to 26 kPa. (b) AFM images of 33Y and 33Y photo-cross-linked peptides. 33Y yields short, single fibers, while photo-cross-linked 33Y self-organizes into a much longer and clustered network of bundled nanofibers.

Looking at their mechanical properties, the viscosity of the photo-cross-linked 33Y was analyzed and compared to that of the untreated 33Y (Fig. S3a†). Both peptides showed non-Newtonian shear-thinning behavior with a decrease of viscosity as the shear-rate increases. However, photo-cross-linked 33Y showed overall increased viscosity values (0.19 Pa s) compared to 33Y alone (0.03 Pa s); this is likely ascribable to the dityrosine cross-links among the peptide nanofiber bundles, providing additional and stronger (covalent links) entanglements at the nanoscale. We next measured the mechanical stiffness of the SAP hydrogels using oscillatory shear rheological experiments. By monitoring the temporal evolution of G' upon addition of neutral pH-buffer, we observed the gelation kinetics and the increasing hydrogel stiffness of both un-cross-linked and photo-cross-linked 33Y peptides (Fig. S3b†). Trends of G' for all peptides showed typical hydrogel-like profiles, suggesting that the glycine linker effectively acts as a spacer, lowering the interference of geometric constraints coming from dityrosine cross-links *vs.* the self-assembly propensity of the LDLK12 backbone. Subsequently, we investigated G′ as a function of angular frequency (1–100 Hz, fixed strain 1% within the LVR) of both 33Y peptides (Fig. 5a). As expected, the 33Y wild type, being a soft hydrogel, displayed an elastic shear modulus of 2 kPa. On the other hand, photo-cross-linked 33Y showed a significantly increased G' throughout the tested frequency range, with values of around 26 kPa. In addition, strain failure tests were performed within the linear viscoelasticity region to assess material failure when subjected to a linear strain progression at +25 °C (Fig. S3c†). In this case failure occurred for both peptides at ∼12% strain.

Lastly, AFM analysis was performed to study the effect of photo-cross-linking on the peptide nanostructures (Fig. 5b). Both the peptides formed nanofibers, with 33Y yielding short single fibers, while photo-cross-linked 33Y showed an increased presence of much longer and clumped fibers. In addition, no changes in the morphology of the nanofibers were observed in both acidic and basic buffers (Fig. S4†). From a morphological point-of-view, ruthenium photo-cross-linking did not hamper 33Y's propensity to self-assemble, but, on the contrary, fostered a "clustering effect" of the self-assembled nanofibers, favoring their pairing and lengthening. From a mechanical perspective, ruthenium photo-cross-linking efficiently increased the stiffness of the 33Y hydrogel and its shear-thinning features, making it useful for 3D printing applications, where SAP-based materials have not yet been fully probed.

3. Conclusions

In this work, we reported the feasibility of ruthenium photo-induced chemical cross-linking on a tyrosine-containing LDLK12 SAP. The peptide sequence has been rationally designed to avoid crosstalk between self-assembly and photo-cross-linking, thus ensuring the effectiveness of ruthenium-complex-catalyzed conversion of tyrosine to dityrosine upon light irradiation. We observed a stable formation of dityrosine cross-linking after 5 minutes with a high fluorescent emission in the visible region. Also, due to the direct deprotonation–protonation process between the ruthenium complex and SAP molecules, the fluorescence of the photo-cross-linked SAP can selectively "turn off" and "turn on" in acid and basic solutions, respectively, while in the presence of sulfuric acid the pH-sensitive switch was inverted. At the same time, this approach enhances the mechanical stability and shear-thinning feature of the peptide-based hydrogel. Altogether, the photo-cross-linking method reported in this work can contribute to new applications of SAP-based biomaterials in biomedical imaging, pH sensing, photonics, soft electronics, and 3D printing.

4. Materials and methods

4.1 Materials

All reagents and solvents used for the peptide synthesis and characterization were purchased from commercial sources and used without further purification.

4.2 General procedure for peptide synthesis and purification

The peptide Ac-YYGGGLDLKLDLKLDLK-$CONH_2$ (dubbed 33Y) was synthesized *via* Fmoc solid-phase peptide synthesis, by

using a Liberty-Discovery (CEM) microwave automated synthesizer. Synthesis was carried out with 0.5 M HBTU in DMF and 2 M DIEA in NMP as activator and activator base solutions, respectively. Fmoc-protected amino acids were dissolved at a concentration of 0.2 M in DMF, and the deprotection solution for Fmoc-group removal was 20% (v/v) 4-methylpiperidine in DMF. A 20% (v/v) solution of Ac_2O in DMF was used for the N-terminal acetylation. Removal of side-chain protecting groups and cleavage was obtained by using a 95 : 2.5 : 2.5 mixture of TFA : TIS : H_2O. Purified peptide powder was dissolved in 0.1 M HCl solution in order to remove the potential presence of TFA salts. Raw peptide was subsequently purified using a Waters binary HPLC apparatus, and the molecular weight was identified *via* single quadrupole mass detection (Waters LC-MS Alliance-3100).

4.3 Photo-cross-linking of hydrogels in the presence of $Ru(bpy)_3Cl_2$ and ammonium persulfate (APS)

Lyophilized 33Y was dissolved in distilled water to achieve a final concentration of 1% (w/v) and then stored at +4 °C overnight. The photo-cross-linked 33Y peptide was prepared by adding $Ru(bpy)_3Cl_2$ (4 μl, 6.25 μM) and APS (2 μl, 178 mM) to a 50 μl pre-assembled solution of 33Y peptide. Then, the mixture was vigorously vortexed and stored for 5 min at room temperature prior to light irradiation with white light (using a 220 W lamp as the light source, $\lambda_{ex} = 452$ nm) for a certain amount of time (*i.e.* 5, 10, 15, 20, 25, and 60 min). Meanwhile, 8 μl of sulfuric acid (H_2SO_4) was added to change the electrochemical and photo-physical properties of $Ru(bpy)_3Cl_2$ (0.18 mg). Afterwards, the photo-cross-linked 33Y peptide was prepared by adding $Ru(bpy)_3Cl_2$–H_2SO_4 (8 μl) and APS (2 μl) to a 50 μl pre-assembled solution of 33Y peptide.

4.4 UV-vis spectroscopy

To monitor the formation of dityrosine crosslinks, solutions of $Ru(bpy)_3Cl_2$ alone (50 μl), 33Y wild type (50 μl, 1% w/v), and photo-cross-linked 33Y (50 μl, 1% w/v) after different light-irradiation times were prepared for UV-vis measurement. The UV-vis spectra (250–800 nm at 25 °C) were recorded on an Infinite M200 PRO plate reader. The background from the solvent was subtracted, and data were processed with Origin™ 8 software.

4.5 Fluorescence spectroscopy

Solutions of $Ru(bpy)_3Cl_2$ alone (50 μl), 33Y wild type (50 μl, 1% w/v), and photo-cross-linked 33Y (50 μl, 1% w/v) after different light-irradiation times were prepared for the fluorescence experiment. The fluorescence intensity was recorded using an Infinite M200 PRO plate reader (Tecan) with $\lambda_{ex} = 280$ nm (5 nm bandpass) and $\lambda_{em} = 380$–800 nm (10 nm bandpass), at 25 °C. Measurements were processed with Origin™ 8 software.

4.6 Absorption and fluorescence spectroscopy at different pHs

Absorption and fluorescence measurements on photo-cross-linked 33Y peptides at different pHs were performed maintaining the same 1% (w/v) final concentration, starting from 2% concentration and adding the same amount in volume of different pH buffers. All samples were measured at room temperature using an Infinite M200 PRO plate reader (Tecan). Measurements were processed with Origin™ 8 software.

4.7 Rheology measurements

The rheological properties of the peptide hydrogels were studied using an AR-2000ex rheometer (TA Instruments) equipped with a truncated cone-plate geometry (acrylic truncated diameter, 20 mm; angle, 1°; truncation gap, 34 μm). The viscosity of the peptide samples was measured using a flow step program, at increasing shear rate, to evaluate the non-Newtonian behavior of the hydrogels. To monitor the sol–gel transition and to evaluate the storage (G') and loss (G'') modulus increase as a function of time, a 10 h time sweep test (constant angular frequency, 1 Hz; fixed strain, 1%) was carried out. Afterwards, to evaluate the G'/G'' moduli of the assembled peptide hydrogels, frequency sweep experiments were conducted as a function of angular frequency (0.1–1000 Hz) at a fixed strain of 1%. Then, a strain sweep test was performed on the samples from 0.01% to 1000% strain to determine the limit of the linear viscoelastic regime (LVR) and, therefore, the maximum strain to which the sample can be tested.

4.8 Atomic Force Microscopy (AFM)

AFM measurements were performed in tapping mode by using a Multimode Nanoscope V system (Digital Instrument, Veeco), using single-beam silicon cantilever probes (Bruker RFESP-75 0.01–0.025 Ohm-cm antimony (n) doped Si, cantilever f_0, resonance frequency 75 kHz, constant force 3 N m^{-1}). The 33Y peptide and photo-cross-linked 33Y peptide were prepared a day prior to imaging. AFM images were taken by depositing a 5 μl drop of peptide solutions (final concentration of 0.01% w/v) onto freshly cleaved mica. The samples were allowed to dry under ambient conditions for 5 min. Subsequently, the samples were rinsed with distilled water to remove loosely bound peptides, and then dried under ambient conditions for 30 min. The images were analyzed and visualized using Nanoscope Software as previously described.[15] The morphological parameter analysis of the AFM data was performed using the Matlab-based open-source software FiberApp, as previously described.[16]

Author contributions

Conceptualization, R. P. and F. G.; methodology, R. P.; software, R. P. and M. M.; validation, R. P.; formal analysis, R. P. and M. M.; investigation, R. P. and M. M.; data curation, R. P.; writing—original draft preparation, R. P. and F. G.; writing—review and editing, R. P. and F. G.; supervision, R. P. and F. G.; funding acquisition, F. G. All authors have read and agreed to the published version of the manuscript.

Conflicts of interest

There are no conflicts to declare.

Acknowledgements

This research was funded by the "Ricerca Corrente 2018–2021" funding granted by the Italian Ministry of Health, by BRIC2019-ID25 granted by INAIL, and by the "5 × 1000" voluntary contributions. Financial support also came from Revert Onlus.

References

1 S. Zhang, Self-assembling peptides: From a discovery in a yeast protein to diverse uses and beyond, *Protein Sci.*, 2020, **29**(11), 2281–2303.
2 F. Gelain, Z. Luo, M. Rioult and S. Zhang, Self-assembling peptide scaffolds in the clinic, *npj Regener. Med.*, 2021, **6**(1), 9.
3 F. Gelain, Z. Luo and S. Zhang, Self-Assembling Peptide EAK16 and RADA16 Nanofiber Scaffold Hydrogel, *Chem. Rev.*, 2020, **120**(24), 13434–13460.
4 R. Pugliese and F. Gelain, Peptidic Biomaterials: From Self-Assembling to Regenerative Medicine, *Trends Biotechnol.*, 2017, **35**(2), 145–158.
5 J. Chen and X. Zou, Self-assemble peptide biomaterials and their biomedical applications, *Bioact. Mater.*, 2019, **4**, 120–131.
6 A. Levin, T. A. Hakala, L. Schnaider, G. J. L. Bernardes, E. Gazit and T. P. J. Knowles, Biomimetic peptide self-assembly for functional materials, *Nat. Rev. Chem.*, 2020, **4**, 615–634.
7 H. Yokoi, T. Kinoshita and S. Zhang, Dynamic reassembly of peptide RADA16 nanofiber scaffold, *Proc. Natl. Acad. Sci. U. S. A.*, 2005, **102**(24), 8414–8419.
8 Y. Zhao, H. Yokoi, M. Tanaka, T. Kinoshita and T. Tan, Self-assembled pH-responsive hydrogels composed of the RATEA16 peptide, *Biomacromolecules*, 2008, **9**(6), 1511–1518.
9 M. P. Hendricks, K. Sato, L. C. Palmer and S. I. Stupp, Supramolecular Assembly of Peptide Amphiphiles, *Acc. Chem. Res.*, 2017, **50**(10), 2440–2448.
10 Z. Yu, F. Tantakitti, T. Yu, L. C. Palmer, G. C. Schatz and S. I. Stupp, Simultaneous covalent and noncovalent hybrid polymerizations, *Science*, 2016, **351**(6272), 497–502.
11 R. Pugliese, A. Marchini, G. Saracino, R. N. Zuckermann and F. Gelain, Cross-linked self-assembling peptide scaffolds, *Nano Res.*, 2017, **11**, 586–602.
12 K. Baek, I. Hwang, I. Roy, D. Shetty and K. Kim, Self-assembly of nanostructured materials through irreversible covalent bond formation, *Acc. Chem. Res.*, 2015, **48**(8), 2221–2229.
13 N. Uchida and T. Muraoka, Current Progress in Cross-Linked Peptide Self-Assemblies, *Int. J. Mol. Sci.*, 2020, **21**(20), 7577.
14 R. Pugliese, M. Maleki, R. N. Zuckermann and F. Gelain, Self-assembling peptides cross-linked with genipin: resilient hydrogels and self-standing electrospun scaffolds for tissue engineering applications, *Biomater. Sci.*, 2018, **7**(1), 76–91.
15 R. Pugliese, L. Moretti, M. Maiuri, T. Romanazzi, G. Cerullo and F. Gelain, Superior mechanical and optical properties of a heterogeneous library of cross-linked biomimetic self-assembling peptides, *Mater. Des.*, 2020, **194**, 108901.
16 R. Pugliese and F. Gelain, Cross-Linked Self-Assembling Peptides and Their Post-Assembly Functionalization *via* One-Pot and *In Situ* Gelation System, *Int. J. Mol. Sci.*, 2020, **21**(12), 4261.
17 L. Calvanese, P. Brun, G. M. L. Messina, T. Russo, A. Zamuner, L. Falcigno, G. D'Auria, A. Gloria, L. Vitagliano, G. Marletta and M. Dettin, EAK Hydrogels Cross-Linked by Disulfide Bonds: Cys Number and Position Are Matched to Performances, *ACS Biomater. Sci. Eng.*, 2020, **6**(2), 1154–1164.
18 K. Sato, W. Ji, L. C. Palmer, B. Weber, M. Barz and S. I. Stupp, Programmable Assembly of Peptide Amphiphile *via* Noncovalent-to-Covalent Bond Conversion, *J. Am. Chem. Soc.*, 2017, **139**(26), 8995–9000.
19 C. Li, A. Iscen, H. Sai, K. Sato, N. A. Sather, S. M. Chin, Z. Alvarez, L. C. Palmer, G. C. Schatz and S. I. Stupp, Supramolecular-covalent hybrid polymers for light-activated mechanical actuation, *Nat. Mater.*, 2020, **19**(8), 900–909.
20 S. Zhang, W. Cortes and Y. Zhang, Constructing Cross-Linked Nanofibrous Scaffold *via* Dual-Enzyme-Instructed Hierarchical Assembly, *Langmuir*, 2020, **36**(22), 6261–6267.
21 L. Chronopoulou, Y. Toumia, B. Cerroni, D. Pandolfi, G. Paradossi and C. Palocci, Biofabrication of genipin-crosslinked peptide hydrogels and their use in the controlled delivery of naproxen, *New Biotechnol.*, 2017, **37**(pt. A), 138–143.
22 I. C. Li and J. D. Hartgerink, Covalent Capture of Aligned Self-Assembling Nanofibers, *J. Am. Chem. Soc.*, 2017, **139**(23), 8044–8050.
23 W. Y. Seow and C. A. Hauser, Tunable mechanical properties of ultrasmall peptide hydrogels by crosslinking and functionalization to achieve the 3D distribution of cells, *Adv. Healthcare Mater.*, 2013, **2**(9), 1219–1223.
24 S. A. H. Hulgan, A. A. Jalan, I. C. Li, D. R. Walker, M. D. Miller, A. J. Kosgei, W. Xu, G. N. Phillips Jr and J. D. Hartgerink, Covalent Capture of Collagen Triple Helices Using Lysine–Aspartate and Lysine–Glutamate Pairs, *Biomacromolecules*, 2020, **21**(9), 3772–3781.
25 I. C. Li, S. A. H. Hulgan, D. R. Walker, R. W. Farndale, J. D. Hartgerink and A. A. Jalan, Covalent Capture of a Heterotrimeric Collagen Helix, *Org. Lett.*, 2019, **21**(14), 5480–5484.
26 L. H. Jones, A. Narayanan and E. C. Hett, Understanding and applying tyrosine biochemical diversity, *Mol. BioSyst.*, 2014, **10**(5), 952–969.
27 B. P. Partlow, M. B. Applegate, F. G. Omenetto and D. L. Kaplan, Dityrosine Cross-Linking in Designing Biomaterials, *ACS Biomater. Sci. Eng.*, 2016, **2**(12), 2108–2121.
28 J. L. Wong and G. M. Wessel, Free-radical crosslinking of specific proteins alters the function of the egg extracellular matrix at fertilization, *Development*, 2008, **135**(3), 431–440.
29 S. O. Andersen, Characterization of a new type of cross-linkage in resilin, a rubber-like protein, *Biochim. Biophys. Acta*, 1963, **69**, 249–262.

30 C. S. Wang, N. N. Ashton, R. B. Weiss and R. J. Stewart, Peroxinectin catalyzed dityrosine crosslinking in the adhesive underwater silk of a casemaker caddisfly larvae, *Hysperophylax occidentalis*, *Insect Biochem. Mol. Biol.*, 2014, **54**, 69–79.
31 J. C. Lennox and J. L. Dempsey, Influence of Proton Acceptors on the Proton-Coupled Electron Transfer Reaction Kinetics of a Ruthenium–Tyrosine Complex, *J. Phys. Chem. B*, 2017, **121**(46), 10530–10542.
32 A. Rajeswari, A. Ramdass, P. Muthu Mareeswaran and S. Rajagopal, Electron Transfer Studies of Ruthenium(II) Complexes with Biologically Important Phenolic Acids and Tyrosine, *J. Fluoresc.*, 2016, **26**(2), 531–543.
33 A. Marchini, A. Raspa, R. Pugliese, M. A. El Malek, V. Pastori, M. Lecchi, A. L. Vescovi and F. Gelain, Multifunctionalized hydrogels foster hNSC maturation in 3D cultures and neural regeneration in spinal cord injuries, *Proc. Natl. Acad. Sci. U. S. A.*, 2019, **116**(15), 7483–7492.
34 D. Cigognini, D. Silva, S. Paloppi and F. Gelain, Evaluation of mechanical properties and therapeutic effect of injectable self-assembling hydrogels for spinal cord injury, *J. Biomed. Nanotechnol.*, 2014, **10**(2), 309–323.
35 J. Kisiday, M. Jin, B. Kurz, H. Hung, C. Semino, S. Zhang and A. J. Grodzinsky, Self-assembling peptide hydrogel fosters chondrocyte extracellular matrix production and cell division: implications for cartilage tissue repair, *Proc. Natl. Acad. Sci. U. S. A.*, 2002, **99**(15), 9996–10001.
36 J. K. Tripathi, S. Pal, B. Awasthi, A. Kumar, A. Tandon, K. Mitra, N. Chattopadhyay and J. K. Ghosh, Variants of self-assembling peptide, KLD-12 that show both rapid fracture healing and antimicrobial properties, *Biomaterials*, 2015, **56**, 92–103.
37 A. Marchini, C. Favoino and F. Gelain, Multi-Functionalized Self-Assembling Peptides as Reproducible 3D Cell Culture Systems Enabling Differentiation and Survival of Various Human Neural Stem Cell Lines, *Front. Neurosci.*, 2020, **14**, 413.
38 A. Caprini, D. Silva, I. Zanoni, C. Cunha, C. Volonte, A. Vescovi and F. Gelain, A novel bioactive peptide: assessing its activity over murine neural stem cells and its potential for neural tissue engineering, *New Biotechnol.*, 2013, **30**(5), 552–562.
39 C. Cunha, S. Panseri and F. Gelain, Engineering of a 3D nanostructured scaffold made of functionalized self-assembling peptides and encapsulated neural stem cells, *Methods Mol. Biol.*, 2013, **1058**, 171–182.
40 F. Gelain, D. Cigognini, A. Caprini, D. Silva, B. Colleoni, M. Donega, S. Antonini, B. E. Cohen and A. Vescovi, New bioactive motifs and their use in functionalized self-assembling peptides for NSC differentiation and neural tissue engineering, *Nanoscale*, 2012, **4**(9), 2946–2957.
41 R. Pugliese, F. Fontana, A. Marchini and F. Gelain, Branched peptides integrate into self-assembled nanostructures and enhance biomechanics of peptidic hydrogels, *Acta Biomater.*, 2018, **66**, 258–271.
42 F. Taraballi, A. Natalello, M. Campione, O. Villa, S. M. Doglia, A. Paleari and F. Gelain, Glycine-spacers influence functional motifs exposure and self-assembling propensity of functionalized substrates tailored for neural stem cell cultures, *Front. Neuroeng.*, 2010, **3**, 1.
43 T. G. Huggins, M. C. Wells-Knecht, N. A. Detorie, J. W. Baynes and S. R. Thorpe, Formation of *o*-tyrosine and dityrosine in proteins during radiolytic and metal-catalyzed oxidation, *J. Biol. Chem.*, 1993, **268**(17), 12341–12347.
44 V. Basavalingappa, S. Bera, B. Xue, J. O'Donnell, S. Guerin, P. A. Cazade, H. Yuan, E. U. Haq, C. Silien, K. Tao, L. J. W. Shimon, S. A. M. Tofail, D. Thompson, S. Kolusheva, R. Yang, Y. Cao and E. Gazit, Diphenylalanine-Derivative Peptide Assemblies with Increased Aromaticity Exhibit Metal-like Rigidity and High Piezoelectricity, *ACS Nano*, 2020, **14**(6), 7025–7037.
45 K. Tao, W. Hu, B. Xue, D. Chovan, N. Brown, L. J. W. Shimon, O. Maraba, Y. Cao, S. A. M. Tofail, D. Thompson, J. Li, R. Yang and E. Gazit, Bioinspired Stable and Photoluminescent Assemblies for Power Generation, *Adv. Mater.*, 2019, **31**(12), e1807481.
46 J. Sakakibara and R. J. Adrian, Whole field measurement of temperature in water using two-color laser induced fluorescence, *Exp. Fluids*, 1999, **26**, 7–15.
47 M. Črnigoj, R. Kostanjšek, G. Kaletunç and N. P. Ulrih, Effect of different fluorescent dyes on thermal stability of DNA and cell viability of the hyperthermophilic archaeon *Aeropyrum pernix*, *World J. Microbiol. Biotechnol.*, 2008, **24**, 2115–2123.
48 L. Li, W. Wang, J. Tang, Y. Wang, J. Liu, L. Huang, Y. Wang, F. Guo, J. Wang, W. Shen and L. A. Belfiore, Classification, Synthesis, and Application of Luminescent Silica Nanoparticles: a Review, *Nanoscale Res. Lett.*, 2019, **14**(1), 190.
49 M. Mirenda, V. Levi, M. L. Bossi, L. Bruno, A. V. Bordoni, A. E. Regazzoni and A. Wolosiuk, Temperature response of luminescent tris(bipyridine)ruthenium(II)-doped silica nanoparticles, *J. Colloid Interface Sci.*, 2013, **392**, 96–101.
50 O. Filevich and R. Etchenique, 1D and 2D temperature imaging with a fluorescent ruthenium complex, *Anal. Chem.*, 2006, **78**(21), 7499–7503.
51 M. K. Brennaman, J. H. Alstrum-Acevedo, C. N. Fleming, P. Jang, T. J. Meyer and J. M. Papanikolas, Turning the $[Ru(bpy)_2dppz]^{2+}$ light-switch on and off with temperature, *J. Am. Chem. Soc.*, 2002, **124**(50), 15094–15098.
52 S. A. McFarland, D. Magde and N. S. Finney, Conformational control of excited-state dynamics in highly distorted Ru(II) polypyridyl complexes, *Inorg. Chem.*, 2005, **44**(11), 4066–4076.
53 T. T. Meng, H. Wang, Z. B. Zheng and K. Z. Wang, pH-Switchable "Off–On–Off" Near-Infrared Luminescence Based on a Dinuclear Ruthenium(II) Complex, *Inorg. Chem.*, 2017, **56**(9), 4775–4779.
54 M. Montalti, S. Wadhwa, W. Y. Kim, R. A. Kipp and R. H. Schmehl, Luminescent ruthenium(II) bipyridyl-phosphonic acid complexes: pH dependent photophysical behavior and quenching with divalent metal ions, *Inorg. Chem.*, 2000, **39**(1), 76–84.
55 F. Liu, K. Wang, G. Bai, Y. Zhang and L. Gao, The pH-induced emission switching and interesting DNA-binding

properties of a novel dinuclear ruthenium(II) complex, *Inorg. Chem.*, 2004, **43**(5), 1799–1806.
56 M. J. Han, L. H. Gao, Y. Y. Lu and K. Z. Wang, Ruthenium(II) complex of Hbopip: synthesis, characterization, pH-induced luminescence "off–on–off" switch, and avid binding to DNA, *J. Phys. Chem. B*, 2006, **110**(5), 2364–2371.
57 Z. B. Zheng, Y. Q. Wu, K. Z. Wang and F. Li, pH luminescence switching, dihydrogen phosphate sensing, and cellular uptake of a heterobimetallic ruthenium(II)–rhenium(I) complex, *Dalton Trans.*, 2014, **43**(8), 3273–3284.
58 H. Shahroosvand, P. Abbasi, A. Faghih, E. Mohajerani, M. Janghouri and M. Mahmoudi, A new class of color-tunable electroluminescent ruthenium(II) phenanthroline emitters, *RSC Adv.*, 2014, (3), 1150–1154.